

**Pulling a harmonically bound particle subjected to Coulombic friction: A nonequilibrium analysis**T. Feghhi , W. Tichy , and A. W. C. Lau*Department of Physics, Florida Atlantic University, Boca Raton, Florida 33431, USA*

(Received 4 May 2022; accepted 27 July 2022; published 11 August 2022)

We address the effects of dry friction, which has emerged only recently to play an important role in some biological systems. In particular, we investigate the nonequilibrium dynamics of a mesoscopic particle, bound to a spring being pulled at a definite speed, moving on a surface with dry friction in a noisy environment. We model the dry friction phenomenologically with a term that is proportional to the sign of the velocity, and by means of numerical simulations of a Langevin equation we show that (a) the frictional force scales with the logarithm of the pulling velocity, (b) the probability distribution function of the spatial displacement away from the potential minimum is non-Gaussian, (c) the fluctuation-dissipation theorem is violated as expected, but (d) the work function obeys the stationary fluctuation theorem, with an effective temperature related to the noise of the system.

DOI: [10.1103/PhysRevE.106.024407](https://doi.org/10.1103/PhysRevE.106.024407)**I. INTRODUCTION**

While Coulombic or dry friction plays an important role for the sliding of macroscopic objects [1], it has only emerged recently in biological systems. For example, leukocyte cells rolling in contact with the endothelium [2] and living cells migrating on viscoelastic substrates [3] exhibit the stick-slip motion, one of the hallmarks of dry friction. At a smaller scale, the movement of kinesin motor protein on microtubules, when it is dragged by a focused laser tweezer, displays nonlinear friction that is consistent with the behavior of dry friction [4]. More recently, the friction between two F-actin filaments has been measured and it is shown to be proportional to the logarithm of the sliding velocity [5]. The latter behavior is again a characteristic of dry friction [6]. What these biological systems show is that the friction at the mesoscopic scales may be dominated by the Coulombic force rather than the viscous force, as we usually assume. Indeed, we can estimate the drag force on a mesoscopic object as  $F_d = 6\pi\mu Rv \approx 10^{-15} N$ , where  $\mu \approx \text{mPa}$  is the dynamic viscosity,  $R \approx \mu\text{m}$  is the linear size of the object, and  $v \approx \mu\text{m/s}$  is the typical speed. On the other hand, the Coulombic friction can be as strong as  $\Delta \approx 10^{-12} N$  [4,5,7]. Thus, to elucidate the statistical description of biological interaction, we must understand the interplay of the Coulombic friction, which is a nonlinear force; the fluctuations arising from the environments, which may not be purely thermal in origin; and the external force such as the harmonic potential as in most experimental setups.

In this paper, we report on a nonequilibrium analysis of a simple model that exhibits interesting behavior under the influence of dry friction and the fluctuations of the environment, but otherwise confined to a harmonic potential. A simple phenomenological model for dry friction was introduced by de Gennes to address the dynamics of granular grains on a vibrating surface [8]. To model the dry friction experienced by the grain and the effect of the vibrating surface, de Gennes

included, respectively, a term that is proportional to the sign of the velocity and a Gaussian white noise into the equation of motion. He showed that there are three different regimes: a viscous, a partly stuck, and a stuck regime [8]. In the partly stuck regime, the velocity distribution is exponential with a “kink” at  $v = 0$ . Subsequently, there has been a number of papers investigating various aspect of the model. In Ref. [9], the authors formulated a path integral approach to understand the stick-and-slip motion. They also calculated the average velocity as a function of an external constant force acting on the particle [10]. In Ref. [11], the authors analyzed the Fokker-Planck (FP) equation not only for the velocity but also for the spatial displacement, the statistics of which exhibit interesting multiscale properties arising from the Coulombic friction.

However, none of these papers deals with the fundamentals of measuring dry friction under experimental settings [4]. We address this problem by exploring, by means of numerical simulations, the nonequilibrium dynamics of a particle subjected to dry friction and noise (not necessarily arising from thermal fluctuations), but otherwise confined to a harmonic potential which pulls the particle at a constant speed (see Fig. 1). Here is a summary of our results.

(1) We show that for a range of velocity, the frictional force scales with the logarithm of pulling velocity, in agreement with recent experimental findings.

(2) We find that the spatial displacement has a non-Gaussian probability distribution function (PDF).

(3) We demonstrate the violation of the fluctuation-dissipation theorem (FDT), which is expected for out of equilibrium system.

(4) Nonetheless, we show that the stationary fluctuation theorem (FT) for work done on the particle holds if we define an effective temperature related to the noise of the system.

This paper is organized as follows: In Sec. II, we introduce the model. In Sec. III, we study the stationary state distribution

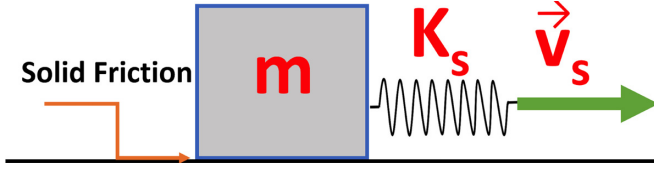


FIG. 1. A mesoscopic particle of mass  $m$  bound to harmonic potential with spring constant  $K_s$ , pulled with a speed  $v_s$  on a surface with Coulombic friction, and subjected to a Gaussian noise from the environment.

of the spatial and velocity component of model. In Sec. IV, we study the frictional force for different noise and pulling speed. In Secs. V and VI, we study the mean square displacement (MSD) and fluctuation dissipation theorem in conjunction with fluctuation theorem for the model.

## II. THE MODEL

The Langevin equation for the setup as depicted in Fig. 1 can be written as

$$m \frac{dv}{dt} = -\Delta \sigma(v) - K_s(x - v_s t) + \eta(t), \quad (1)$$

$$\mathbf{J}_r = \begin{pmatrix} v'P \\ -(K_s/m)x'P - (\Delta/2m)[\sigma(v' + v_s) + \sigma(-v' + v_s)]P \end{pmatrix}, \quad (3)$$

and an irreversible part,

$$\mathbf{J}_{ir} = \begin{pmatrix} 0 \\ -(\Delta/2m)[\sigma(v' + v_s) - \sigma(-v' + v_s)]P - (g^2/m^2) \partial_{v'} P \end{pmatrix}. \quad (4)$$

Under time reversal,  $t \rightarrow -t$ , the position and the velocity components of reversible  $\mathbf{J}_r$  (irreversible  $\mathbf{J}_{ir}$ ) current are transformed in the same (opposite) way as the time derivative of  $x'$  and of  $v'$ , respectively.

An equilibrium system, in addition to being time independent, i.e.,  $\partial_t P = 0$ , satisfies the condition of detailed balance, which dictates that  $\mathbf{J}_{ir}$  must vanish [12,13]. This gives an equation for the equilibrium phase distribution, which can be readily solved. However, this solution does not satisfy the stationary state condition  $\nabla \cdot \mathbf{J}_r = 0$ , unless  $K_s$  is identically zero [13]. This implies that a harmonically bound particle under dry friction and noise is intrinsically out of equilibrium. Nevertheless, the system does possess a stationary state, and most of our results are obtained in this regime.

## III. STATIONARY STATE DISTRIBUTIONS

In this section, we present the PDFs from the numerical simulation of Eq. (1). First, for simplicity, we scale out a characteristic length,  $\ell \equiv \Delta/K_s$ , and a time,  $\tau \equiv \sqrt{m/K_s}$ , so that  $\tilde{x} = x'/\ell$ ,  $\tilde{t} = t/\tau$ , and  $\tilde{v} = (\tau/\ell) v'$ . The scaled Langevin equation only depends on two parameters,  $\tilde{v}_s = v_s(\tau/\ell)$  and  $\tilde{g} = g/(\Delta\sqrt{\tau})$ . We employ the Euler scheme with convergence of order 1 to integrate Eq. (1) forward in time [14,15]. The probability distribution,  $P(\tilde{v}, \tilde{x})$ , is obtained by binning the phase space from a trajectory generated by running the

code for  $\approx 10^6 \tau$ , which, we believe, is sufficient time to establish steady state [16].

where  $x$  is the position of the particle and  $v = dx/dt$  is its velocity. The dry friction is modeled by  $-\Delta\sigma(v)$ , where  $\Delta$  is the strength and  $\sigma(x)$  is the sign function, defined as  $\sigma(v) = 1$  for  $v > 0$ ,  $\sigma(v) = -1$  for  $v < 0$ , and  $\sigma(v) = 0$  for  $v = 0$ . The third term represents the harmonic potential moving at speed  $v_s$  and  $K_s$  is the spring constant. The last term  $\eta(t)$  represents the stochastic force arising from the fluctuations of the environment, modeled by a Gaussian white noise, i.e.,  $\langle \eta(t) \rangle = 0$  and  $\langle \eta(t)\eta(t') \rangle = 2g^2\delta(t-t')$ , where  $g$  represents the strength of the noise.

To show that the dynamics of this system described by Eq. (1) is intrinsically out of equilibrium, we first derive the corresponding FP equation. Introducing the comoving frame, defined by  $x' = x - v_s t$  and  $v' = v - v_s$ , we obtain

$$\partial_t P = -\partial_{x'}(v'P) + m^{-1} \partial_{v'} \{ [\Delta \sigma(v' + v_s) + K_s x'] P \} + (g^2/m^2) \partial_{v'}^2 P, \quad (2)$$

where  $P(v', x', t)$  is the phase-space distribution function of the particle as a function of  $t$ . Note that this equation, as in any FP equation, can be written as  $\partial_t P = -\nabla \cdot \mathbf{J}$ , which expresses conservation of probability. The current  $\mathbf{J}$  consists of two parts [12]: a reversible part

We find it visually more appealing to report  $P(\tilde{v})$  and  $P(\tilde{x})$ , obtained by binning, respectively,  $\tilde{v}$  and  $\tilde{x}$  from the trajectories of Eq. (1). The results are plotted in Fig. 2 for different values of  $\tilde{v}_s$  at a fixed  $\tilde{g}$ . First, a striking feature of  $P(\tilde{v})$  is the sharp nondifferentiable point (singularity) for all  $\tilde{g}$  and  $\tilde{v}_s$  at  $\tilde{v} = 0$ . The singularity, which is also present without the spring, arises from the discontinuity of the sign function in Eq. (1) [8,17]. When the particle is being pulled at a low velocity, there appears another maximum in  $P(\tilde{v})$  near  $\tilde{v} \approx \tilde{v}_s$ . As the pulling speed increases, this peak becomes more pronounced and eventually it corresponds to the most probable speed. Physically, at low pulling speed, the particle does not have enough momentum to overcome dry friction and becomes stuck momentarily, but at some point the linearly increasing force sets the particle into motion, in short jumps. At a higher pulling speed, the particle starts to slide more frequently, therefore its most probable speed becomes roughly  $\tilde{v}_s$ . Also, we note that increasing  $\tilde{v}_s$  broadens the width of the peak at  $\tilde{v} = \tilde{v}_s$ . Interestingly, the two peaks, one at  $\tilde{v} = 0$  and the other at  $\tilde{v} = \tilde{v}_s$  coexist for a large range of  $\tilde{v}_s$ . Increasing the strength of the effective noise  $\tilde{g}$  causes the transition from single peak to double peak to happen at larger pulling speed.

For the displacement of the particle  $\tilde{x}$  away from the bottom of the potential, we find that, despite being a harmonic

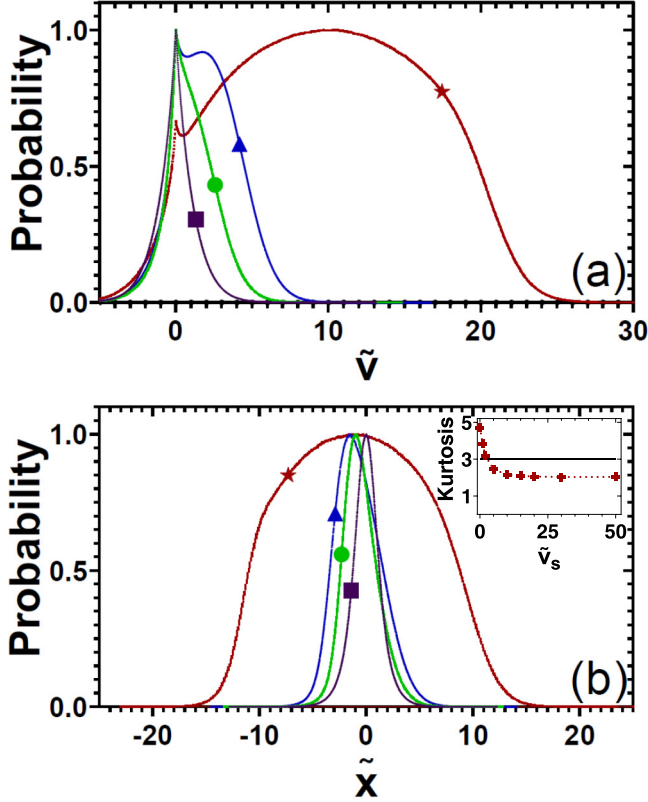


FIG. 2. The stationary state phase space distribution  $P(\tilde{v}, \tilde{x})$  as obtained from numerical simulations of Eq. (1) for  $\tilde{g} = 1$  where  $\tilde{x} = x'/\ell$ ,  $\tilde{v} = (\tau/\ell)v'$ , and  $\tilde{g} = g/(\Delta\sqrt{\tau})$ . (a) The normalized velocity distribution in the laboratory frame  $P(\tilde{v})/P_M$  [where  $P_M$  is the maximum of  $P(\tilde{v})$  and  $P(\tilde{v}) \equiv \int d\tilde{x} P(\tilde{v}, \tilde{x})$ ] for different values of  $\tilde{v}_s$ . From the left,  $\tilde{v}_s = 0$  ( $\square$ ), 1 ( $\circ$ ), 2 ( $\triangle$ ), and 10 ( $\star$ ). The sharp peak at  $\tilde{v} \approx 0$  for all values of  $\tilde{v}_s$  shown is a signature of dry friction. However, as  $\tilde{v}_s$  increases, there appears a secondary maximum, roughly at  $\tilde{v} \sim \tilde{v}_s$ , corresponding to the object sliding due to the force from the spring. Increasing  $\tilde{v}_s$  increases the magnitude of the peak and  $\tilde{v}_s$  becomes the most probable speed. (b) The normalized spatial distribution in the comoving frame  $P(\tilde{x}) \equiv \int d\tilde{v} P(\tilde{v}, \tilde{x})$  for different values of  $\tilde{v}_s$  [same legends as in (a)]. Note that the distribution is not Gaussian in  $\tilde{x}$ ; this can be seen from the inset of (b) which shows the kurtosis of  $P(\tilde{x})$  vs  $\tilde{v}_s$  for  $\tilde{g} = 1$ . While the calculated skewness is small, the kurtosis starts out at roughly 5 for  $\tilde{v}_s = 0$ , and goes asymptotically to 2 as  $\tilde{v}_s$  increases. For comparison, a purely Gaussian distribution has a kurtosis of 3 (solid line) and uniform distribution has a kurtosis of 1.8.

potential,  $P(\tilde{x})$  is not Gaussian, as shown in Fig. 2(b). This non-Gaussianity is likely arising from the nonlinear nature of the dry friction. To characterize the non-Gaussianity of the distribution  $P(\tilde{x})$ , we can measure its skewness and kurtosis. A purely Gaussian distribution has a kurtosis and a skewness of three and zero, respectively. In our case, the skewness is roughly zero and the kurtosis is not 3, as shown in the inset of Fig. 2(b). For low pulling velocities, the kurtosis is determined to be more than 3 and decreases to 2 for large pulling velocities. Another interesting feature of  $P(\tilde{x})$  is that the most probable value of  $\tilde{x}$ , i.e., the value of  $\tilde{x}$  at which  $P(\tilde{x})$  is a maximum, decreases as  $\tilde{v}_s$  increases. This is related to the

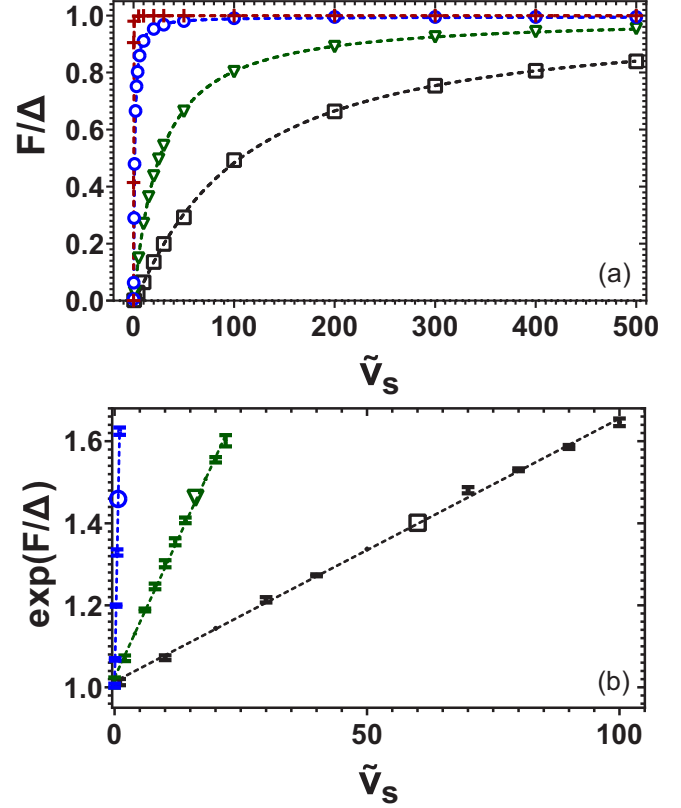


FIG. 3. Frictional force, as obtained from  $F = K_s \langle x' \rangle = \Delta \langle \tilde{x} \rangle$  as a function of the pulling velocity,  $\tilde{v}_s$ , for increasing values of  $\tilde{g} = 0.1$  (+), 1 ( $\circ$ ), 5 ( $\triangle$ ), 10 ( $\square$ ). When fluctuations are weak, the force curve resembles a step function, but as  $\tilde{g}$  increases, the force scales sublinearly for small  $\tilde{v}_s$  and asymptotically goes to a constant for large  $\tilde{v}_s$  given by  $\Delta$ . (b) The force vs pulling velocity curve as in (a) but plotted in a linear-log scale [same legends as in (a)], showing that the force scales with  $\tilde{v}_s$  as  $\ln \tilde{v}_s$  for sufficiently large  $\tilde{g}$ . This scaling is a signature of dry friction. The error bars represent the standard deviation of simulations [15].

counteracting force due to the harmonic potential to balance out the Coulombic friction. Note that this also happens for the case with viscous friction, except that the most probable value of  $\tilde{x}$  decreases linearly with increasing  $\tilde{v}_s$ . For the case of Coulombic friction, the most probable value of  $\tilde{x}$  approaches to a constant value as the pulling velocity gets larger, as expected.

#### IV. FRICTIONAL FORCE AS A FUNCTION OF PULLING VELOCITY

One of the motivations to study the dynamics of the system depicted in Fig. 1 is that it represents a typical experimental setup to measure friction, where the harmonic potential is generated by an optical tweezer [4]. In a statistical steady state, the force from the spring balances that of the dry friction on the average. Therefore, the friction force is given by  $F = K_s \langle x' \rangle = \Delta \langle \tilde{x} \rangle$ , which is a function of pulling speed,  $\tilde{v}_s$ . The average is calculated directly from the time series of the  $\tilde{x}(t)$  in the simulation. The results are plotted in Fig. 3. At low  $\tilde{g}$ , we are in the deterministic limit, where  $\langle \tilde{x} \rangle = \sigma(\tilde{v}_s)$ . However,

at higher  $\tilde{g}$ , the magnitude of force initially increases with the pulling speed, the slope of which decreases as  $\tilde{g}$  increases. We can interpret this behavior as follows: In the deterministic limit, pulling the object at a constant speed, the average of applied force must equal the Coulombic friction. However, increasing the effective noise makes the particle move with constant speed even with an applied force (on average) smaller than Coulombic force of the contact surface. In other words, the solid friction is effectively softened. In fact, as can be seen in Fig. 3(b), there is a range of the pulling velocity  $\tilde{v}_s$ , in which the frictional force scales with the logarithm of the pulling velocity. This scaling is a signature of dry friction, and has been predicted with microscopic models and confirmed experimentally [5]. It is interesting to obtain this here using a phenomenological model. This scaling arises from the activation process in a noisy environment. In our case, when the particle is being pulled, the system has two states: a stuck phase with  $\tilde{v} \approx 0$  and a sliding phase with  $\tilde{v} \approx \tilde{v}_s$ . Note that in transition from stuck phase to sliding phase, the particle needs to move faster than  $\tilde{v}_s$  to catch up with the moving spring. The noise in the system might occasionally kick the system from a stuck to the sliding phase. Therefore, assuming that the Kramers law [12] is valid for this system,  $\langle v \rangle \sim \exp(-F/g^2)$ , which implies that  $F \sim \ln v_s$ .

### V. MEAN-SQUARED DISPLACEMENT AND THE VIOLATION OF THE FLUCTUATION-DISSIPATION THEOREM

Another interesting quantity that shows the interplay between diffusion property and dry friction is the MSD of the particle, defined as  $\bar{d}^2(t) = \langle [\tilde{x}(t) - \tilde{x}(0)]^2 \rangle$ , where the average represents the average over noise as well as time average. In Fig. 4, we plot our numerical results for the MSDs, in which we identify two distinct behaviors of the particle—a diffusive regime which occurs at both small  $\tilde{g}$  and small pulling velocity,  $\tilde{v}_s$ , and an underdamped regime for large  $\tilde{g}$  and  $\tilde{v}_s$ , as shown in the inset of Fig 4(b). We should note that this behavior is different from a similar system with viscous force only, in that its behavior does not depend on  $\tilde{v}_s$ .

In the diffusive regime, the MSD rises as time increases and flattens to an asymptotic value of  $2[\langle \tilde{x}^2 \rangle - \langle \tilde{x} \rangle^2]$ , which is the width of the distribution. In the underdamped regime, the MSD exhibits oscillatory motion. Interestingly, the higher the pulling  $\tilde{v}_s$ , the more oscillatory is the MSD. This is expected because as  $\tilde{v}_s$  increases, we are increasing the energy of the system and the particle essentially exhibits deterministic motion.

Next, we discuss the FDT, which is a cornerstone of equilibrium statistical mechanics; it posits that, at equilibrium, the correlation function,  $C(t-s)$ , of an observable is linked to its response function,  $R(t-s)$ , via  $\partial_s C(t-s) = k_B T R(t-s)$ , where  $k_B$  is Boltzmann's constant and  $T$  is the temperature. Here, the linear response function is defined as  $R(t-s) \equiv \langle \delta x(t) / \delta f(s) \rangle$  for the variable  $x(t)$  in response to an external force  $f(t)$ . Among its many applications, the FDT allows one to measure the correlation function to back out some information encoded in the response function about the dissipative process of the system [18].

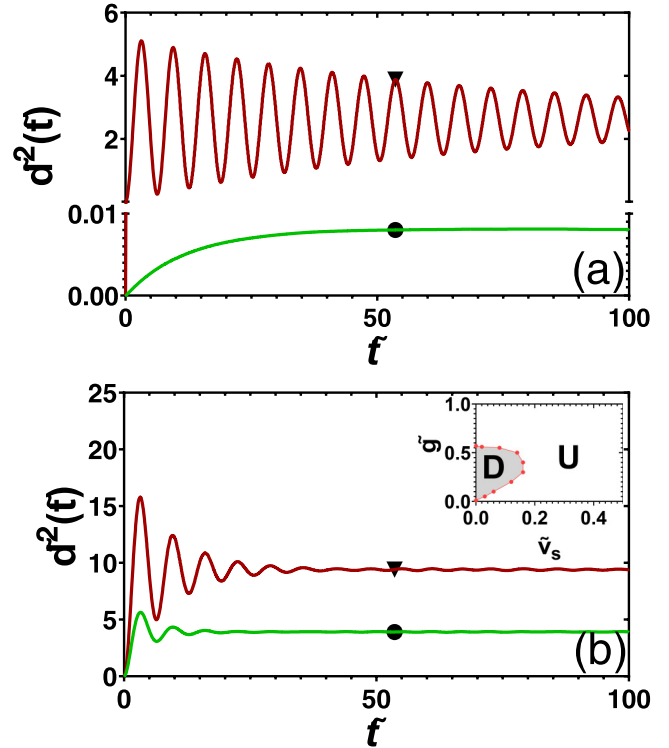


FIG. 4. The mean-squared displacement as a function of time for  $\tilde{g} = 0.2$  (a) and  $\tilde{g} = 1$  (b) for  $\tilde{v}_s = 0$  ( $\circ$ ) and  $\tilde{v}_s = 2$  ( $\nabla$ ). At low  $\tilde{g}$ , the MSD resembles the motion of the particle in the deterministic limit: at low  $\tilde{v}_s$ , the particle is in the diffusive regime, but at high  $\tilde{v}_s$ , the particle exhibits oscillatory motion. At high  $\tilde{g}$ , MSD resembles that of a damped harmonic oscillator in the underdamped limit. Note that in both cases, increasing  $\tilde{v}_s$  increases the amplitude of the oscillation. Inset of (b): A phase diagram showing the region in the parameter space in which the particle exhibits diffusive (D) and underdamped (U) behaviors. The regions are obtained by visually inspecting the behavior of MSD at a particular  $\tilde{g}$  and  $\tilde{v}_s$ . If the MSD monotonically increases to a constant value, we consider it as diffusive (D). On the other hand, if the MSD exhibits oscillations we consider it as underdamped (U). We note that only for a small range of  $\tilde{g}$  and  $\tilde{v}_s$  we have diffusive motion. The system crosses over the underdamped regime by increasing  $\tilde{g}$  and  $\tilde{v}_s$ . Red points represent roughly the boundary of the diffusive and underdamped regimes.

However, as shown earlier, our system is intrinsically out of equilibrium and we expect the FDT to be violated because of continuous dissipation of energy as indicated by a nonzero irreversible current of our system. However, it would be interesting to see if a FDT-like relation could still hold when an effective temperature is properly defined [19]. To that end, we take the average kinetic energy to be an effective temperature, i.e.,  $(1/2)k_B T_{\text{eff}} = (m/2)\langle v^2 \rangle = (\Delta^2/2K_s)\langle \tilde{v}^2 \rangle$ , and we plot, from our numerical simulations,  $2k_B T_{\text{eff}} \text{Im} \chi(\omega)$  versus  $\omega C(\omega)$ , where  $C(\omega)$  and  $\chi(\omega)$  are the Fourier transform of  $C(t-s)$  and  $R(t-s)$ , respectively [20] in scaled units. If FDT holds, then all data points would collapse onto a straight line with a slope of 1. The results are plotted in Fig. 5, where we display our numerical results for four representative cases: two cases in which the pulling velocity is zero and two cases

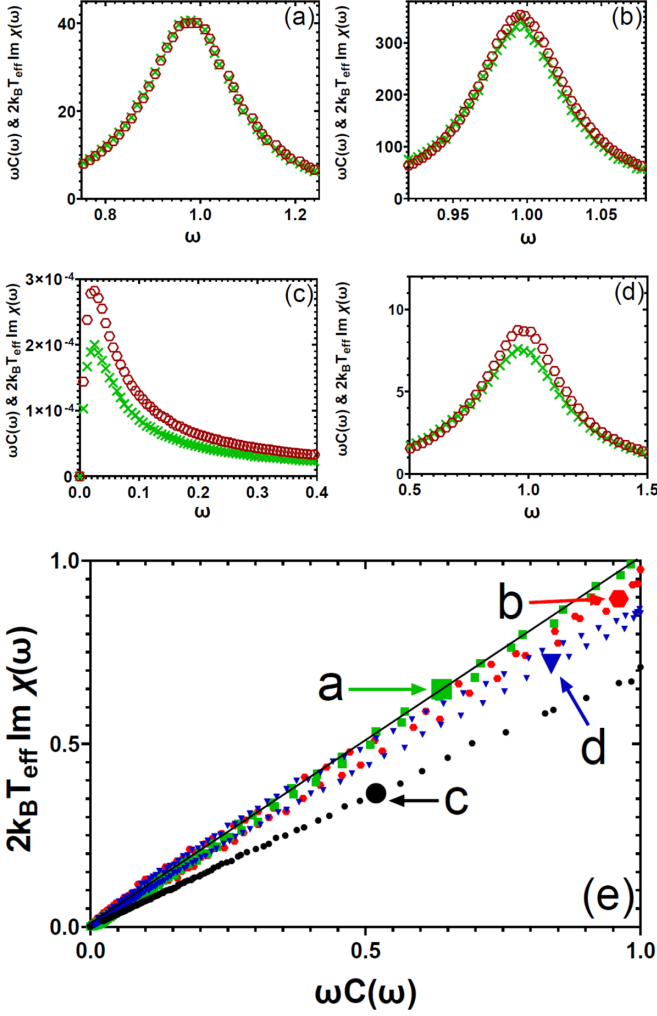


FIG. 5. Plots of the Fourier transform of the linear response function  $k_B T_{\text{eff}} \text{Im} \chi(\omega)$  ( $\times$ ) and correlation function  $\omega C(\omega)$  ( $\circ$ ) for different values of  $\tilde{g}$  and  $\tilde{v}_s$ , where  $T_{\text{eff}}$  represents the effective temperature. Here, case a corresponds to  $(\tilde{g} = 1, \tilde{v}_s = 2)$ , case b corresponds to  $(\tilde{g} = 1, \tilde{v}_s = 5)$ , case c corresponds to  $(\tilde{g} = 0.1, \tilde{v}_s = 0)$ , and case d corresponds to  $(\tilde{g} = 1, \tilde{v}_s = 0)$ . For a fluctuation-dissipation theorem to hold,  $\omega C(\omega)$  and  $2k_B T_{\text{eff}} \text{Im} \chi(\omega)$  must overlap. For case a, at this particular  $\tilde{g}$  and  $\tilde{v}_s$ , the FDT is obeyed. For cases b–d, the FDT is violated. However, for case c, the FDT can be restored with a redefinition of the effective temperature, about  $1.4 \times T_{\text{eff}}$ . (e) A plot of the response function  $2k_B T_{\text{eff}} \text{Im} \chi(\omega)$  vs the correlation functions  $\omega C(\omega)$  for cases a (■), b (●), c (●), and d (▼), as indicated. Note that the response function and the correlation functions have been normalized by the maximum values of  $\omega C(\omega)$  for each cases. For a fluctuation-dissipation-like theorem to hold, the slope would be 1, as indicated by the solid black line. We also observe that cases b and d are not single valued, implying a frequency dependent temperature.

in which the system is driven, i.e., the pulling velocity is not zero.

When the system is not driven, i.e.,  $\tilde{v}_s = 0$ , the FDT is indeed violated for both low and high  $\tilde{g}$  regimes. For these cases, the correlation functions and response functions are displayed in cases c and d in Fig. 5. For low  $\tilde{g}$ , which is the diffusive regime [see inset of Fig. 4(b)], a FDT-like relation

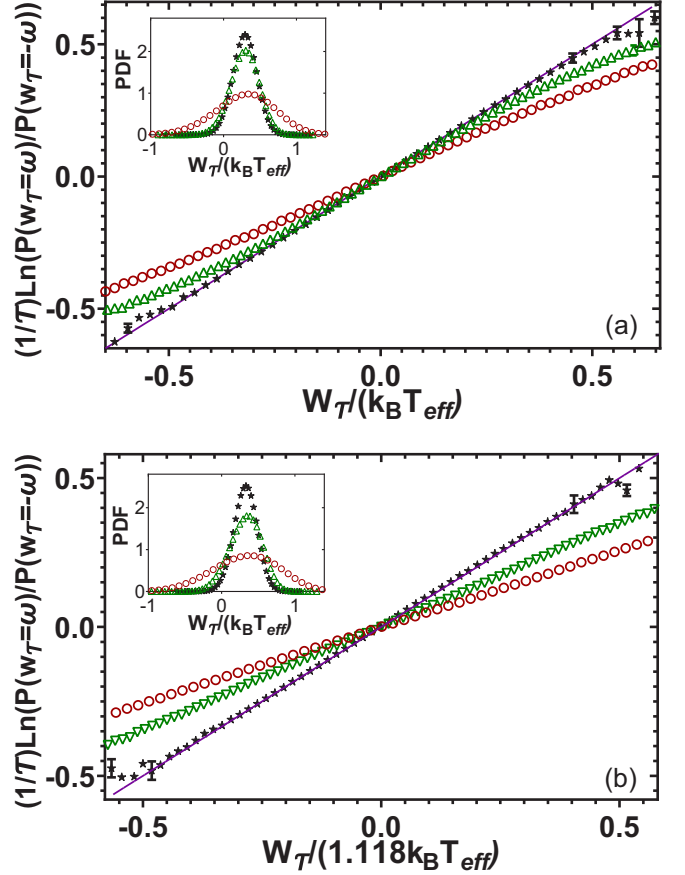


FIG. 6. Fluctuation theorem for the time-averaged work done (over a time period  $\mathcal{T}$ ) on the particle:  $W_{\mathcal{T}} \equiv -(K_s/\mathcal{T}) \int_0^{\mathcal{T}} dt' (x - v_s t') v_s$ . We plot from our numerical simulations,  $\mathcal{T}^{-1} \ln[P(W_{\mathcal{T}} = w)/P(W_{\mathcal{T}} = -w)]$  vs  $W_{\mathcal{T}}/(k_B T_{\text{eff}})$  for (a)  $(\tilde{g} = 1, \tilde{v}_s = 2)$ , and (b)  $(\tilde{g} = 1, \tilde{v}_s = 5)$ , at three different values of  $\mathcal{T}/\tau = 5$  ( $\circ$ ), 15 ( $\triangle$ ), and 20 ( $\star$ ), where  $\tau \equiv \sqrt{m/K_s}$ . The error bars indicate the standard deviation of simulations and for most of the points it is smaller than the symbols used [15]. We should note that the parameters for (a) and (b) correspond to the cases in which the FDT holds or does not, hold, respectively (see Fig. 5). To verify the stationary state FT, the value of  $\mathcal{T}$  should be large enough. When increasing the value of  $\mathcal{T}$ , the slope of (a) approaches 1, while for (b) it is 0.84. Thus, the FT holds for (a) but for (b) it holds only if we redefine  $T_{\text{eff}}$ , as 1.188 times the average kinetic energy of the particle. Insets: The probability distribution of work  $W_{\mathcal{T}}$  for different values of  $\mathcal{T}$ .

can be restored if we choose an effective temperature that is different from  $T_{\text{eff}}$  above. The exact value of this temperature is greater than  $T_{\text{eff}}$  and approaches  $T_{\text{eff}}$  as  $\tilde{g}$  increases to the boundary of the diffusive regime.

At an even higher  $\tilde{g}$  in the underdamped regime, not only the FDT is violated, but also if we insist on having a FDT-like relationship, a frequency dependent temperature must be introduced. This can be seen in Fig. 5(d), where the ratio of  $\text{Im} \chi(\omega)$  and  $\omega C(\omega)$  is no longer single valued due to the asymmetry in the ratio of  $\text{Im} \chi(\omega)$  and  $\omega C(\omega)$  around  $\omega = 1$ . For example, at  $\omega = 0.57$  and 1.37, the value of the correlation function  $\omega C(\omega)$  is roughly the same (about 2.05), but the response function  $\text{Im} \chi(\omega)$  at

$\omega = 1.37$  has a value of 1.9 that is smaller than that of  $\omega = 0.57$  which is 2.2. Therefore, they appear to be double valued in Fig. 5(e).

When the system is driven, there is a small range of  $\tilde{v}_s$  at a particular  $\tilde{g}$ , in which a FDT-like relation with an effective temperature so defined holds [see Fig. 5(a)]. However, if the pulling velocity is increased, the FDT is violated again [see Fig. 5(b)].

## VI. FLUCTUATION THEOREM

Recently, the FT has emerged as a useful tool to characterize fluctuations of a system that is driven out of equilibrium. It provides a precise quantitative statement about the probability of a dissipative quantity  $\bar{\sigma}_t$ , such as the entropy production rate or the rate at which work is being done, and states that [21]

$$\lim_{t \rightarrow \infty} \frac{1}{t} \ln \frac{P(\bar{\sigma}_t = A)}{P(\bar{\sigma}_t = -A)} = A, \quad (5)$$

where  $P(\bar{\sigma}_t = A)$  is the probability that  $\bar{\sigma}_t$  has a value  $A$ . It attempts to characterize these fluctuations in far-from-equilibrium regimes where linear response theory fails. FT has been extensively investigated for the problem of a particle attached to a moving spring and subjected to viscous friction and thermal fluctuations [22–24].

Here, we examine the FT associated with the work done on a particle experiencing Coulombic friction. Following Ref. [25], we define the rate at which work is being done on the particle as the work required to keep the potential moving, and write  $W_{\mathcal{T}} = -(K_s/\mathcal{T}) \int_t^{t+\mathcal{T}} dt' (x - v_s t') v_s$ . Note that this definition of work implies that it vanishes identically when the pulling velocity is zero. In the inset of Fig. 6, we plot the probability distribution for  $W_{\mathcal{T}}$  for different values of  $\mathcal{T}$  for two different cases. It is interesting to note that despite the displacement  $\tilde{x}$  having a non-Gaussian distribution (see Fig. 2),  $W_{\mathcal{T}}$  is Gaussian distributed for sufficiently large values of  $\mathcal{T}$ . Furthermore, it is clear that for a given  $\mathcal{T}$ , the probability of having “negative” work  $W_{\mathcal{T}} < 0$  is fi-

nite, but increasing  $\mathcal{T}$  results in a higher probability for the system of having “positive” work  $W_{\mathcal{T}} > 0$ . In both cases, the average of  $W_{\mathcal{T}}/\mathcal{T}$  for all the values of  $\mathcal{T}$  is  $K_s \langle x' \rangle v_s$ , as it should be.

To verify the conventional steady-state FT for  $W_{\mathcal{T}}$ , we plot  $\mathcal{T}^{-1} \ln[P(W_{\mathcal{T}} = w)/P(W_{\mathcal{T}} = -w)]$  versus  $w/(k_B T_{\text{eff}})$  in Fig. 6 for two cases: one in which FDT holds and the other one in which FDT does not. For the first case, the FT holds for large values of  $\mathcal{T}$  with the effective temperature  $T_{\text{eff}}$ . However, for the second scenario, the FT only holds at large  $\mathcal{T}$  if we redefine  $T_{\text{eff}}$ . Increasing  $\mathcal{T}$  further does not change the slope in both cases. Therefore, we have verified for a model of dry friction, which is intrinsically out of equilibrium, that the steady-state FT holds, provided  $\mathcal{T}$  is sufficiently large, even though FDT does not hold, as previously demonstrated.

## VII. CONCLUSION

We have numerically explored a simple model in which the effects of Coulombic friction and a harmonic potential are taken into account for a mesoscopic particle moving in a noisy environment. This problem corresponds to the typical experimental setup, in which friction is being measured quantitatively. For a range of pulling velocity, our model gives a frictional force that scales with the logarithm of the pulling velocity. This behavior is typically observed experimentally. We have also investigated the nonequilibrium properties of the model. In particular, we demonstrate that the model obeys a form of the fluctuation theorem, despite the fact that it is intrinsically out of equilibrium as demonstrated by the violation of the fluctuation-dissipation theorem. We hope that these results give insights into those experiments that measure friction, such as microbalance experiments.

## ACKNOWLEDGMENTS

We thank Prof. Jeffrey Sokoloff for many fruitful discussions. W.T. is supported by NSF Grants No. PHY-2011729 and No. PHY-2136036.

- 
- [1] B. N. J. Persson, *Sliding Friction: Physical Principles and Applications*, 2nd ed. (Springer, New York, 2000).
  - [2] M. Urbakh, J. Klafter, D. Gourdon, and J. Israelachvili, *Nature (London)* **430**, 525 (2004).
  - [3] P. S. De and R. De, *Phys. Rev. E* **100**, 012409 (2019).
  - [4] V. Bormuth *et al.*, *Science* **325**, 870 (2009).
  - [5] A. Ward *et al.*, *Nat. Mater.* **14**, 583 (2015).
  - [6] C. Aumeier *et al.*, *Nat. Cell Biol.* **18**, 1054 (2016).
  - [7] J. Schnauß, T. Golde, C. Schuldt, B. U. Schmidt, M. Glaser, D. Strehle, T. Handler, C. Heussinger, and J. A. Kas, *Phys. Rev. Lett.* **116**, 108102 (2016).
  - [8] P.-G. D. Gennes, *J. Stat. Phys.* **119**, 953 (2005).
  - [9] A. Baule *et al.*, *Nonlinearity* **24**, 351 (2011).
  - [10] H. Touchette *et al.*, *J. Phys. A: Math. Theor.* **45**, 395002 (2012).
  - [11] A. M. Menzel and N. Goldenfeld, *Phys. Rev. E* **84**, 011122 (2011).
  - [12] H. Risken, *The Fokker-Planck Equation* (Springer-Verlag, Berlin, 1989).
  - [13] A. Sarracino, *Phys. Rev. E* **88**, 052124 (2013).
  - [14] P. E. Kloeden, E. Platen, and H. Schurz, *Numerical Solution of SDE Through Computer Experiments* (Springer-Verlag, Berlin, 1994).
  - [15] We used Euler’s scheme to integrate Eq. (1) forward in time with time step  $d\tilde{t} \approx 10^{-6}$  and ran the program at least for  $N \approx 10^{12}$  steps. The white noise is generated by the GSL Mersenne Twister random Gaussian generator with an average of zero and a variance of  $2\tilde{g}^2 d\tilde{t}$ . To check our code, we compared the results of the simulations with the analytical solution to a few cases [11]. In addition, we also numerically solved the FP equation [26,27], Eq. (2), for the probability distribution  $P(\tilde{v}, \tilde{x})$  and compare it to the one obtained from Langevin simulations. In all of these cases, the PDFs from Langevin exactly match with

- FP method and known analytical expressions. The PDFs did not change by replacing the  $\sigma(\tilde{v})$  with  $\tanh(\tilde{v}/\epsilon)$  where  $\epsilon < 10^{-4}$ .
- [16] To check that we are in fact in a stationary state, we also numerically solve Eq. (2), and the result for  $P(\tilde{v}, \tilde{x})$  agrees with that obtained from Eq. (1). In addition, by increasing the number of steps threefold, the resulting PDFs obtained from either Eqs. (1) or (2) do not change. Therefore, we believe that for the region of the parameter space that we have explored in this paper, the system is in a stationary state.
- [17] H. Hayakawa, *Physica D* **205**, 48 (2005).
- [18] P. M. Chaikin and T. C. Lubensky, *Principles of Condensed Matter Physics* (Cambridge University, New York, 1995).
- [19] T. Speck and U. Seifert, *Europhys. Lett.* **74**, 391 (2006).
- [20] In our simulations, we calculate the response function  $R(t - s)$  in two ways. In one method, we compute  $R(t - s) \equiv \langle \delta x(t) / \delta f(s) \rangle$ , where we choose the magnitude of  $f$  to be as small as  $f/\Delta = 0.005$  to ensure that it is in the linear response regime. In a second method, we calculate the response function by the formula,  $R(t - s) = (2g^2)^{-1} \langle x'(t)\eta(s) \rangle$  [28,29]. We have checked that both methods yield the same results.
- [21] D. J. Evans and D. J. Searles, *Adv. Phys.* **51**, 1529 (2002).
- [22] R. van Zon and E. G. D. Cohen, *Phys. Rev. E* **69**, 056121 (2004).
- [23] G. M. Wang, E. M. Sevick, E. Mittag, D. J. Searles, and D. J. Evans, *Phys. Rev. Lett.* **89**, 050601 (2002).
- [24] F. Douarche, S. Joubaud, N. B. Garnier, A. Petrosyan, and S. Ciliberto, *Phys. Rev. Lett.* **97**, 140603 (2006).
- [25] E. G. D. Cohen and R. Van Zon, *C. R. Phys.* **8**, 507 (2007).
- [26] Y. Chen and X. Deng, *Phys. Rev. E* **98**, 033302 (2018).
- [27] Y. Chen and W. Just, *Phys. Rev. E* **90**, 042102 (2014).
- [28] L. Caprini *et al.*, *Symmetry* **13**, 81 (2021).
- [29] E. A. Novikov, *J. Exptl. Theor. Phys. (U.S.S.R.)* **47**, 1919 (1964) [*Sov. Phys. JETP* **20**, 1290 (1965)].